# EXPERIMENTAL INVESTIGATION OF HEAT TRANSFER PHENOMENON OF ANNULAR HEAT PIPE FOR PASSIVE IN-CORE COOLING SYSTEM

**In Guk Kim, Kyung Mo Kim, Yeong Shin Jeong, In Cheol Bang***
School of Mechanical and Nuclear Engineering
Ulsan National Institute of Science and Technology (UNIST)
50 UNIST-gil, Ulju-gun, Ulsan Metropolitan City 689-798, Republic of Korea
icbang@unist.ac.kr

## ABSTRACT

The concept of a hybrid control rod is proposed for a passive in-core cooling system (PINC) for decay heat removal in a pressured water reactor (PWR). The concept aims to combine the roles of heat pipes and control rods in a PWR system. For effective application, the proposed hybrid rod is to be composed of a suitable neutron absorbing material, such as boron carbide, while providing for sufficient heat dissipation. The annular shape of the boron carbide pellets in the heat pipe provides a path for the working fluid. The objective of this paper is to investigate heat transfer performance across these annular spaces. A small scale heat pipe (L: 300 mm, O.D.: 12.7 mm) is analyzed and wall temperature distributions, overall heat transfer, heat transfer coefficients, and capillary limit are determined. Results show a heat transfer reduction due to face friction at the vapor and liquid boundary layers. Theoretical capillary limit of annular flow path heat pipe was slightly lower than concentric heat pipe and then both of predictions were underestimated compared to the experimental results. The liquid pressure drop was dominant for capillary limit, thus the cross-sectional area of vapor space had a low effect on heat pipe dry-out phenomenon. Experimental results indicate that the inner structure of the heat pipe has some effects on performance. It is also confirmed that the annular heat pipe concept of passive decay heat removal works sufficiently.

**KEYWORDS**
Hybrid heat pipe, Heat pipes, Passive IN-core Cooling system (PINCs)

## 1. INTRODUCTION

Heat pipes in nuclear reactor are passive heat transfer device that uses phase change to conduct thermal energy away from the core. Per unit volume, heat pipes have excellent performance for PWR applications, providing uniform heat removal. They are powerful tools for heat removal applications or as a heat transport medium at regions of high thermal energy. Consequently, heat pipes for nuclear power plants applications have been studied for passive decay heat removal system or simply as a general system enhancement. Wang et al. [1] suggested a passive residual heat removal system (PRHRS) for a molten salt reactor (MSR) using sodium heat pipes. Additionally, the transient performance of a high

* Corresponding author: Tel:+82-52-217-2915, Fax:+82-52-217-3008
E-mail : icbang@unist.ac.kr (In Cheol Bang)

temperature sodium heat pipe was numerically simulated for an MSR accident. Jouhara et al. [2] suggested a new concept for a nuclear desalination system based on heat pipe technology. The use of heat pipe based heat recovery systems in desalination plants is expected to improve the overall system performance of the desalination process. Mochizuki et al. [3] proposed a passive cooling system using heat pipes for spent nuclear fuel. Mochizuki et al. [4] suggested heat pipes for nuclear systems that use loop heat pipes for decay heat removal cooling system. These various applications were studied to determine the respective cooling performance of the heat pipes.

Heat pipes have been widely used in various fields including solar energy CPU cooling, and small scale heat transfer applications. Because of increasing demands in cooling performance, the need for more effective cooling system has led to intensive studies of heat pipes using nano-particles and in modifications of wick structures. Kole and Dey [5] studied the synthesis, thermal conductivity, and the thermal performance of screen mesh wick heat pipes using water-based copper nano-fluids. It was found that the thermal performance of the nano-fluid based heat pipe was predominately affected by a layer of Cu nano-particles at the evaporator section. Schampheleire et al. [6] investigated the gravity-assisted orientation heat pipe using three different wicks; screen mesh wick, sintered powder wick and outperforms the fibres wick. Metal fibres wick showed the greatest potential as a wick material for high performance heat pipes. Maziuk et al. [7] developed software for flat, miniature heat pipe based on numerical analysis. Experimental verification confirmed the accuracy of the software.

The concept of a hybrid heat pipe was suggested as a Passive In-core Colling System (PINCs) for decay heat removal for advanced nuclear power plant (Figure 1). It attempts to combine the rules of heat pipes and control rods. It is necessary for PINCs to comprise a neutron absorber material such as $B_4C$. PINCs is to have annular vapor space dimensions and heat transfer reduction in comparison with conventional heat pipes. Control rods in APR-1400 (Korea pressurized water reactor) are typically Inconel 625, 18.7 mm in diameter and filled with mostly neutron absorbent materials. Figure 2 shows the schematic of the hybrid heat pipe design with control rods as PINCs. The working fluid path and wick structure can be achieved using the enrichment of $B^{10}$ and $B_4C$ pellets resulting in an annular vapor flow path of decreased cross-sectional area as compared to concentric heat pipes of equivalent outer diameter. Faghri and Thomas [8] described the concentric annular heat pipe design, testing, and theoretical capillary limit prediction. The main objective was to compare the performance of the concentric annular heat pipe to that of a conventional heat pipe. The difference between the annular vapor space as well as the heat transfer area due to additional surface area is seen in the two designs. The capillary limit of the annular heat pipe dramatically increased resulting in a performance advantage. Faghri [9] indicated that the results are due to the difference in the cross sectional shape, with one circular and the other annular. Lastly, Table I summarizes previous studies on experimental investigations of heat pipes of various geometries.

This paper focuses on the investigation into the heat transfer performance of annular flow path heat pipes with various structures as well as confirming the effects of $B_4C$ pellets in control rod. Annular flow path heat pipes included cylindrical structure of acrylonitrile butadiene styrene (ABS) instead of $B_4C$ from fused deposition. The effects of the cylindrical structure on heat pipe performance and changes in thermal performance were analyzed.

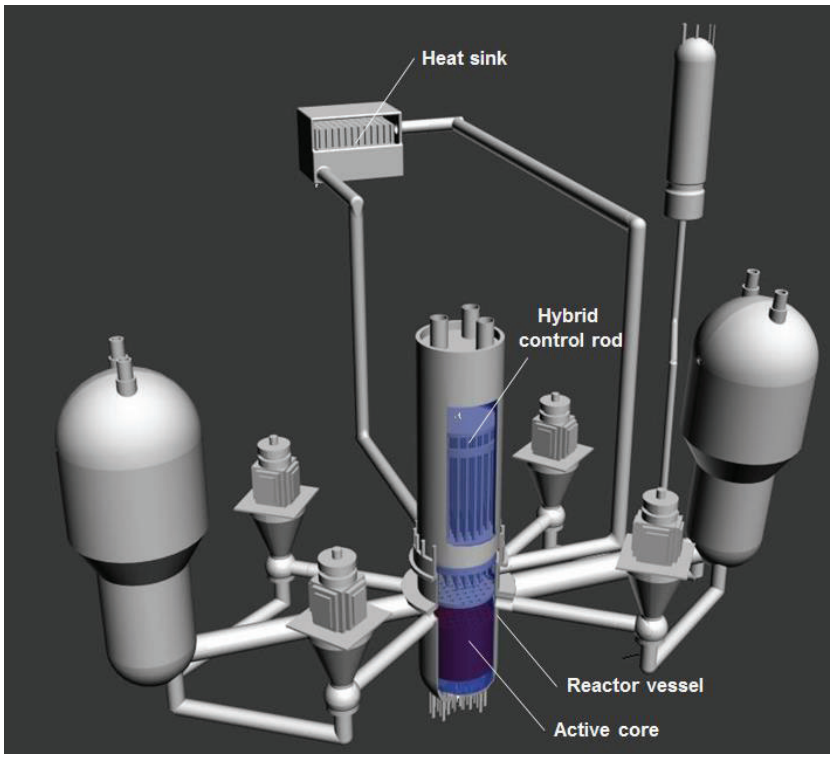


**Figure 1. A Design of Passive In-core Cooling System (PINCs)**

**Table. I Review of heat pipe experimental studies.**

| | Researchers | Working fluids | Temperature range | Wick | Geometry | Types |
|---|---|---|---|---|---|---|
| [8] | A. Faghri (1989) | Water | - 100 °C | Copper groove wick | 300 : 473 : 200 Diameter : 30 (mm) | Annular heat pipe |
| [10] | D.H. Kim et al. (2004) | Water | 40 – 160 °C | Mesh wick (80) | 60 : 80 : 60 Diameter : 25.4 (mm) | Annular heat pipe |
| [11] | J.H. Boo et al. (2005) | Water | 40 - 180 °C | Mesh wick (80) | N/A Diameter : 25.4 (mm) | Annular heat pipe |
| [12] | Y.M. Hung and Q'bert Seng (2011) | Water | 20 – 100 °C | Groove wick | 127 : 246 :127 Diameter : - | Concentric heat pipe |
| [13] | L.G. Asirvatham et al. (2012) | Silver nanoparticles dispersed in DI water | 25 – 160 °C | Copper mesh wick (100) | 50 : 50 : 80 Diameter : 10 ( mm) | Concentric heat pipe |
| [14] | X. Yang et al. (2012) | water | 10 – 90 °C | Groove wick | 362 Diameter : 5 (mm) | Concentric heat pipe |
| [15] | J. Zhang et al. (2013) | δ-$Al_2O_3$-R141b nanofluids | 24 – 40 °C | Groove wick | 140 : 60 : 140 (array) 30 * 2 (mm) | Flat heat pipe |

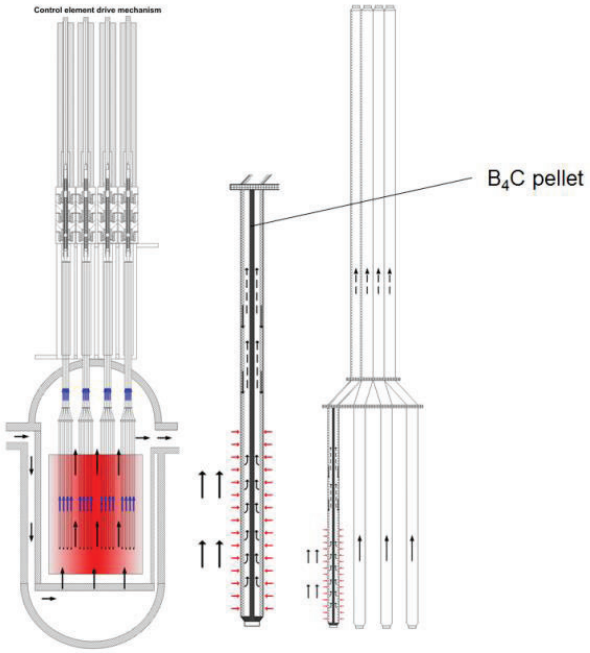


**Figure 2. Schematic Design of the Hybrid Heat Pipe with Control Rod as PINCs**

## 2. EXPERIMENTAL SETUP AND PROCEDURE

### 2.1. Experimental Setup

The experimental heat pipe comprised two layers of stainless steel screen wire mesh as the wick structure with distilled water as the working fluid. Thermal performance of the heat pipe was tested at vertical orientation at various heat loads. The stainless steel 316L test section had an outer diameter of 12.7 mm, an inner diameter of 11.7 mm and a length of 300 mm. The test section had an evaporator region of 100 mm that was heated by direct current copper electrodes. The adiabatic region of 100 mm was insulated with glass wool. The condenser section was 100 mm in length. Its role was to cool the working fluid, maintaining a constant temperature. Six K-type thermocouples were installed to measure the wall temperature along the test section. Two thermocouples were attached to the outer wall of the evaporator region. Two thermocouples measured the outer temperature of the condenser region. Thermocouples were attached to the adiabatic region as well. The uncertainty in the measurement of temperature is $\pm$ 0.6°C. Thermocouple locations as well as a schematic view of the experimental system are shown in Figure 3.
Before filling the system with the working fluid, all non-condensable gas was removed using a vacuum pump. The fluid charge was determined based on the void volume in the wick structure. Distilled water was added to the evaporator section at a 100% fill ratio. A pressure gage was placed at the top of the condenser section to measure the initial saturation pressure as well as the operating pressure of the steam in the heat pipe. Uncertainty of filling ratio due to instrumental error was less than ±5%. The inlet temperature of the coolant was maintained constant with the use of a chiller. The heat load ranged from 45 W to 105 W.

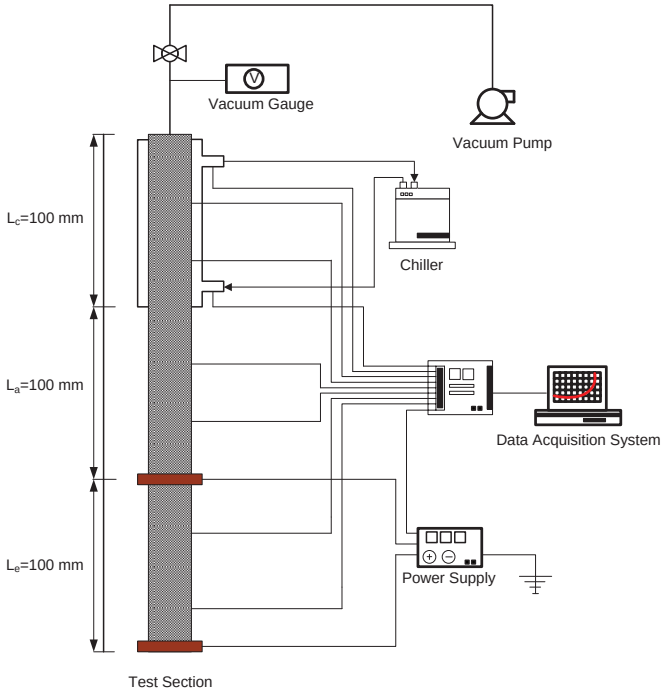


**Figure 3. Schematic Diagram for the Experimental Apparatus**

### 2.2. Test Section Geometry

The test section consisted of a tube made of stainless steel 316L with a stainless steel 304, 100 mesh wick insert. The length, outer diameter, and thickness of the heat pipe were 300 mm, 12.7 mm, and 1.0 mm, respectively. Figure 4 shows the geometry of the heat pipe test section with flow direction indicated. Figure 4 (a) shows a conventional concentric heat pipe (CHP) with evaporation and condenser sections. Both (b) annular evaporator section heat pipe (AEHP) and (c) annular flow path heat pipe (AHP) were of cylindrical structures made of ABS using fused deposition modeling. The length and diameter of the cylindrical structure in the AEHP design are 100 mm and 6.05 mm, respectively. The length and diameter of the cylindrical structure in the AHP design are 300 mm and 6.05 mm, respectively. The conditions of heat pipes were summarized in Table II.

**Table II: Initial conditions**

| Initial Condition | Test |
|---|---|
| Filling ratio | 100 % in wick |
| Wick size | 100 mesh |
| Porosity | 0.62 |
| Vacuum | 8.0 kPa |

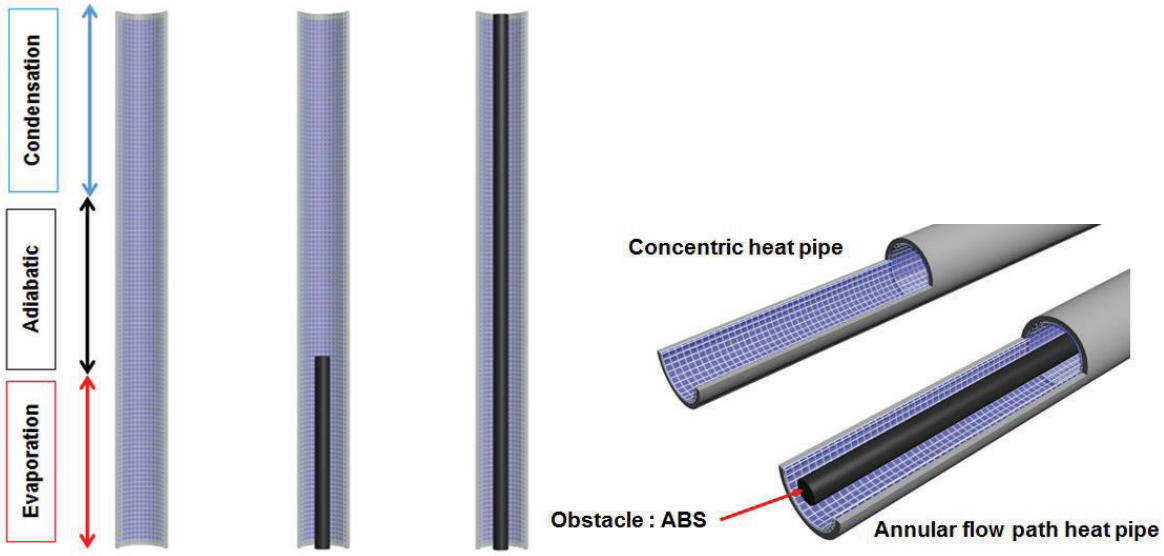


**a) CHP (b) AEHP (c) AHP**

**Figure 4. Test Sections (a) Concentric Heat Pipe, (b) Annular Evaporator Section Heat Pipe, (c) Annular Flow Path Heat Pipe**

### 2.3. Material

ABS is a thermoplastic polymer resulting in a plastic with a lustrous and impervious surface. ABS is easy to fabricate because of its low melting point, approximately 105 °C. ABS and $B_4C$ have similar wettability and specific heat properties on the surface and both materials are insoluble in water. Structures in heat pipe have can have of vapor flow. The main reason in using the ABS material was low thermal conductivity and simple manufacture. The length of tested heat pipes was shorter than control rod ( 0.3 m and 4.4 m, respectively). The concern of small heat pipe test was the conduction through obstacle material (instead of $B_4C$). If the obstacle has similar thermal conductivity, the heat transfer can be dominated by conduction through the obstacle, not by boiling of working fluid. Boiling heat transfer occurs on the inner surface of stainless tubes not ABS material. The existing region of the ABS is vapor flow region, which means ABS material gives no effect on the boiling heat transfer. Figure 5 shows the water-wetting surface with contact angle. $B_4C$ and ABS pellets have a contact angle about 66.2° and 59.1°, respectively. Additional properties of the two materials are summarized in Table III.

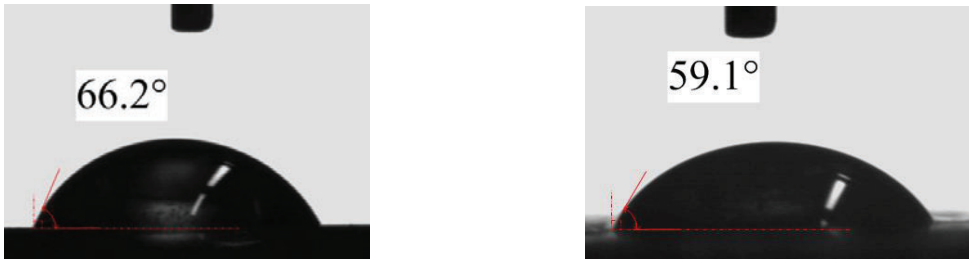


(a) (b)

**Figure 5. Contact Angles (a) Boron Cabide ($B_4C$) Pellet and (b) ABS Pellet**

**Table III: Pellet properties of $B_4C$ and ABS pellet**

| | $B_4C$ pellet | ABS pellet |
|---|---|---|
| Density, g/cm$^3$ | 1.84 | 1.06 – 1.25 |
| Thermal conductivity, W/mK | 3.30 (irradiated) | 0.6 |
| Specific heat, J/kgK | 950 - 1288 | 1100 - 1486 |
| Solubility in water | Insoluble | |
| Contact angle, °C | 66.2 | 59.1 |

## 3. RESULTS AND DISCUSSIONS

### 3.1. Temperature Distributions

The temperature response to heat load of the three heat pipes is shown in Figure 6. The heat input power at the evaporator section was increased incrementally from 45 to 105 W in steps of 20 W. The temperatures of the evaporator and the condenser remained unchanged at each heat load. When a heat power of 110 W was applied, temperature oscillations of evaporator region started and temperature peaks due to the capillary limit were observed. Adiabatic temperatures slightly increased because of internal pressure changes of the heat pipe. The initial pressure of heat pipes was 8 kPa and experimental heat pipes had an operating pressure that ranged from 8.0 kPa to 9.5 kPa. The vapor temperature range of the experimental heat pipes was from 42 °C to 45 °C. Temperature difference between the evaporator sections was approximately 1.5 °C because of heat conduction through the stainless steel structure.

The temperature distribution of the three heat pipes at a 100 % filling ratio is shown in Figure 7. When the heat input of the copper electrode heater was increased, the temperature difference between the evaporator and the condenser section wall also increased. For all power ranges, the AEHP design had the poorest performance. Vaporization of the evaporator section was not enough to transport the working fluid from the evaporator to the condenser at tested temperature range. The AHP design had similar results, but this is attributed to the increased cooling surface per unit volume of vapor due to the annular flow path at the condenser. Additionally, the capillary pumping power of the wick structure is not sufficient to transfer the working fluid from the evaporator to the condenser. The vapor velocity of the AEHP and AHP designs is faster than that of the CHP design. High vapor velocity in heat pipes results in elevated boundary layer friction between the vapor and liquid flows.

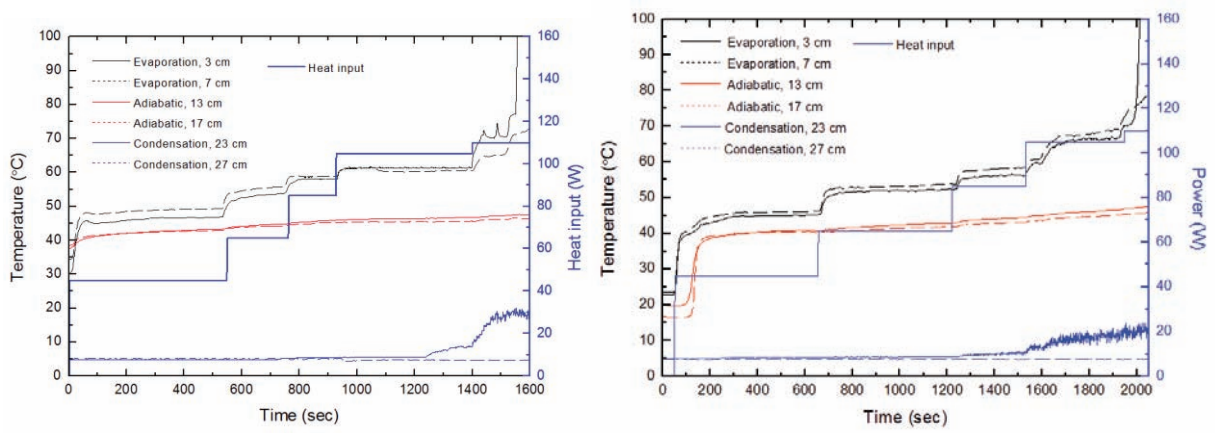


**(a)** **(b)**

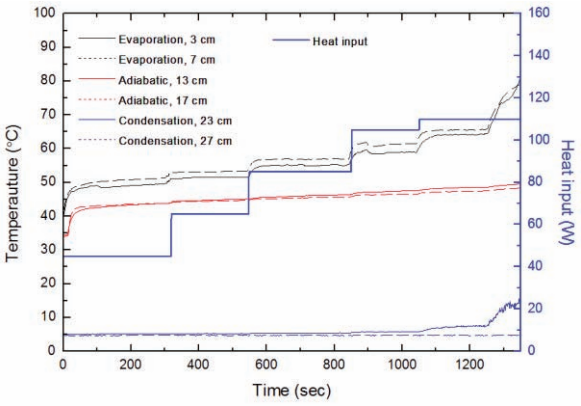


**(c)**

**Figure 6. Temperature Response to Heat Load of (a) Concentric Heat Pipe, (b) Annular Evaporator Section Heat Pipe, (c) Annular Flow Path Heat Pipe**

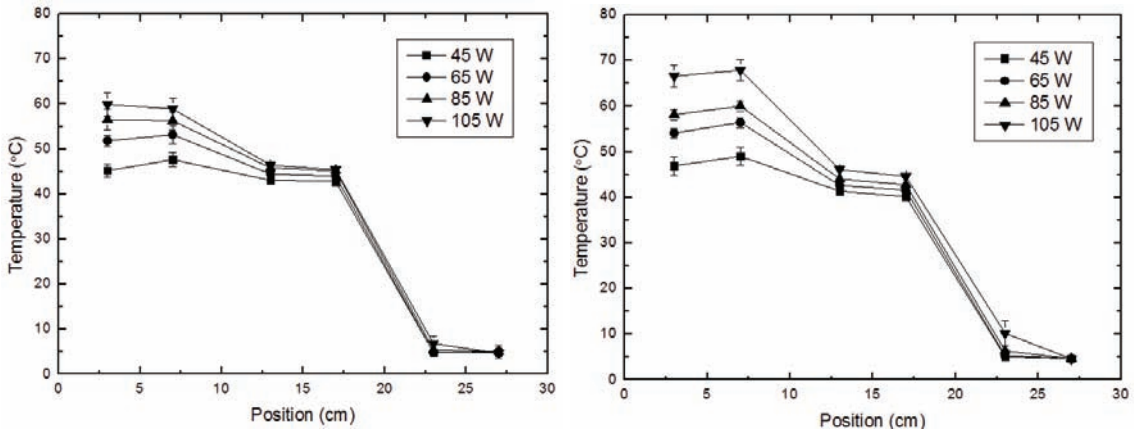


(a) CHP (b) AEHP

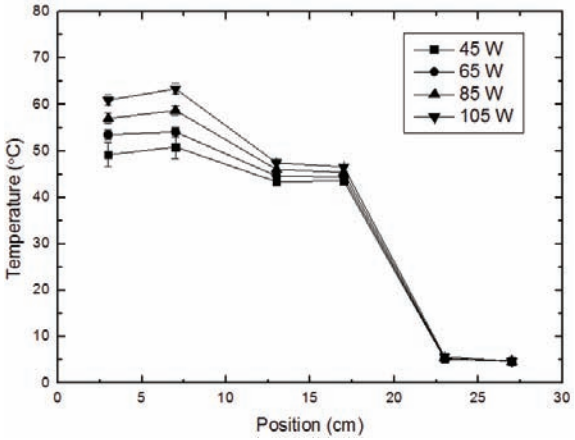


(c) AHP

**Figure 7. Temperature Distribution of Tested Heat Pipes According to Heat Input**

### 3.2. Thermal Resistances and Heat Transfer Coefficients

Figure 8 shows the overall thermal resistance that is plotted as function of the heat input. The thermal resistance of heat pipes shows a trend similar to the experimental results presented by Asirvatham et al. [13] and Shukla et al. [16]. Tested heat pipes show a decreasing thermal resistance with the increase of the heat input. The reduction in thermal resistances of screen mesh wick heat pipes is due to the activation of larger number of nucleation sites in the evaporator surface that increases the regime of nucleate boiling according to heat flux. In figure 9, the overall heat transfer coefficient of tested heat pipes is plotted as function of heat flux. The heat transfer coefficient values from 450 W/m$^2$°C to 820 W/m$^2$°C for the CHP and the values of others are reduced by 2 to 12 % with various heat fluxes. Heat fluxes inputs ranging from 17 kW/m$^2$ to 45 kW/m$^2$. Thermal resistance and heat transfer coefficient can be presented by

$$R_o\left(^\circ C/W\right)=\frac{\overline{T}_e-\overline{T}_c}{Q_e} \tag{1}$$

$$h_o\left(W/m^2{}^\circ C\right)=\frac{q''_e}{\overline{T}_e-\overline{T}_c} \tag{2}$$

The maximum error of the input power is about 0.5%. The uncertainties in overall resistance and heat transfer coefficient are calculated by :

$$\frac{\Delta R_o}{R_o}=\sqrt{\left(\frac{\Delta Q_{in}}{Q_{in}}\right)^2+\left(\frac{\Delta(\Delta T)}{\Delta T}\right)^2} \tag{3}$$

$$\frac{\Delta h_o}{h_o}=\sqrt{\left(\frac{\Delta q''_{in}}{q''_{in}}\right)^2+\left(\frac{\Delta(\Delta T)}{\Delta T}\right)^2} \tag{4}$$

The estimated maximum uncertainties in the thermal resistance and heat transfer coefficient are 6.4 % and 5.1 %, respectively.

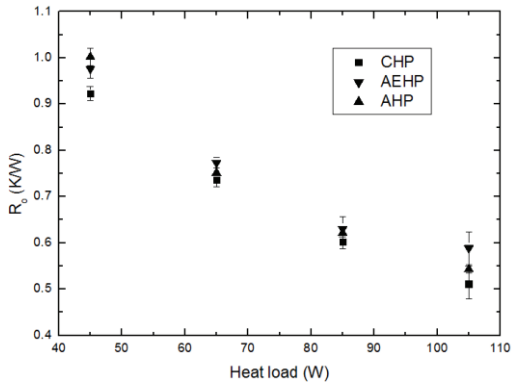


**Figure 8. Overall Heat Resistance of Heat Pipes according to The Heat Load.**

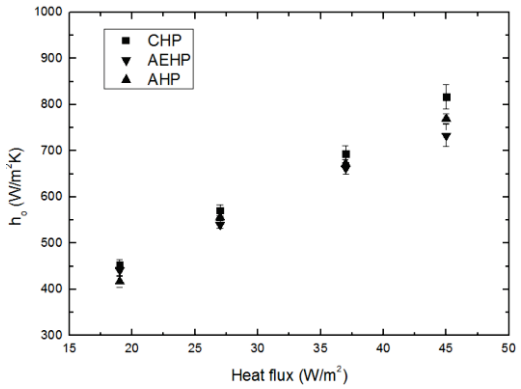


**Figure 9. Overall Heat Transfer Coefficient of Heat Pipes according to The Heat Flux.**

### 3.3. Operation limit of heat pipes

In this section a simple analysis for the prediction of annular flow path heat pipe limit will be presented. It showed the effect of cross-sectional area of vapor and modified correlation for suggested heat pipe geometry. The operation limit of heat pipe is developed using one dimensional approach.

A heat load is applied to bottom of heat pipe, and a heat sink is applied to the top of heat pipe from the schematic of a concentric annular flow path heat pipe. Vaporization occurs in evaporation section due to the heat load and vapor is transferred to condensation section. It is condensed to fluid and absorbed by the wick structure which is highly porous media. The condensed working fluid returns to evaporator section by capillary wicking of wick structure. The driving force for working fluid is affected by capillary and gravitational force. For correct operation of heat pipe,

$$\Delta P_{c,\max} \geq \Delta P_l + \Delta P_v + \Delta P_g \quad (5)$$

If the capillary pressure is smaller than overall pressure drop in heat pipe, the wick will drop out in the evaporation region and the heat pipe will not work. The capillary limit is defined as the maximum allowable heat flux when the heat pipe does not operate. The pressure drop, $\Delta P_{c,\max}$ , is the capillary limit from the wick structure.

Gravitational assisted heat pipe has the hydrostatic head of liquid that is possible to positive or negative, depending on the relative positions of the condensation section and evaporation section. The bottom heated concentric heat pipe has negative value because of the angle, $\phi$ , between the heat pipe and the horizontal. The pressure difference from hydrostatic head is determined from

$$\Delta P_g = \rho_l g l \sin\phi \quad (6)$$

The void fraction of mesh wick is used as the fluid flow path of working fluid. The total flow cross-sectional area, $A_f$ is defined by

$$A_f = \pi(r_w^{\,2} - r_v^{\,2})\varepsilon \quad (7)$$

If the working fluid in heat pipe is constant viscosity and incompressible conditions at given working temperature, the mass flow rate of liquid flow is described from Hagen-Poiseulle equation [17].

$$\dot{m}_l = \rho\pi r^2 v = \frac{\pi(r_w^{\,2} - r_v^{\,2})\varepsilon r_{pore}^2 \rho_l}{8\mu_l}\frac{\Delta P_l}{l_{eff}} \quad (8)$$

Heat transport occurs from heated liquid to vapor phase during the operation of heat pipes, then heat and mass flow is defined as a relation between the latent heat of vaporization and mas flow rate.

$$\dot{Q} = \dot{m}L \quad (9)$$

Rearrangement of Eq. 5,

$$\Delta P_l = \frac{S_1 \mu \dot{Q} l_{eff}}{\pi (r_w^2 - r_v^2) \varepsilon r_e^2 \rho_l L} \tag{10}$$

The vapor pressure difference is defined as the sum of heat pipe sections.

$$\Delta P_v = \Delta P_{v,e} + \Delta P_{v,a} + \Delta P_{v,c} \tag{11}$$

If the pressure drop of vapor is Incompressible and laminar flow, the vapor pressure drop of heat pipe can be modeled by an equation presented by Cotter and Busse [18]. It considered the pressure drop in the vapor phase of long concentric heat pipe therefore it is necessary to modify the correlation. The cross section of annular flow path of heat pipe is defined by

$$A_v = \pi (r_v^2 - r_c^{\,2}) \tag{12}$$

It is suggested the modified correlation for annular flow path heat pipe that is shown in Eq. 11.

$$\Delta P_v = S_2 \frac{\dot{m}}{\rho_v A_v^2} + S_3 \frac{\pi \mu_v \dot{m} l_a}{\rho_v A_v^2} \tag{13}$$

The capillary limit for annular flow path heat pipe is given by the following equation.

$$\Delta P_{c,\max} \geq S_1 \frac{\mu \dot{Q} l_{eff}}{\pi (r_w^2 - r_v^2) \varepsilon r_{pore}^2 \rho_l L} + S_2 \frac{\dot{m}}{\rho_v A_v^2} + S_3 \frac{\pi \mu_v \dot{m} l_a}{\rho_v A_v^2} + \rho_l g l \sin\phi \tag{14}$$

The capillary limit determines the maximum allowable heat flux from the pressure drop in heat pipes. Using a Darcy's law and rearranging,

$$\Delta P_{c,\max} \geq \frac{\mu_l l_{eff} \dot{m}}{\rho_l K A_w} + S_1 \frac{\dot{m}}{\rho_v A_v^2} + S_2 \frac{\mu_v \dot{m} l_a}{\rho_v A_v^2} + \rho_l g l \sin\phi \tag{15}$$

$$\dot{Q} = m_{\max} L = \frac{L}{r_e} (2\sigma_l \cos\theta - \rho_l g l r_e \sin\phi) \left( \frac{1}{\frac{\mu_l l_{eff}}{\rho_l K A_w} + \frac{S_1 + S_2 \mu_l l_a}{\rho_v A_v^2}} \right) \tag{16}$$

The experimentally determined capillary limits of concentric heat pipes were compared with the analytical predictions. The analytical operation limits were determined for adiabatic temperatures from temperature distribution. Operation limits of water based heat pipe were highly related to viscous limit, capillary limit, and boiling limit. In the experimental results, the capillary limit is the dominant limit for the experimental operation temperature. The operation limits of heat pipe are shown in figure. 10.

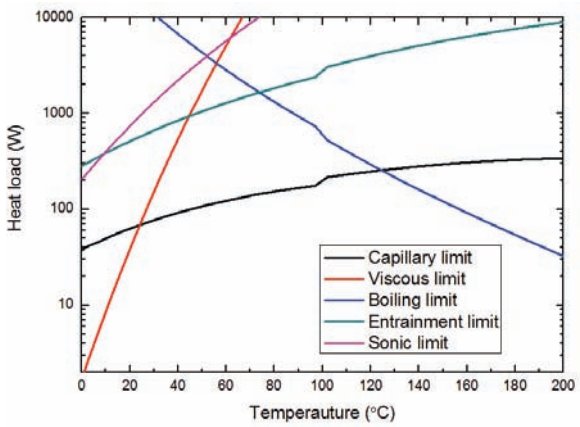


Figure. 10 Operation limit of concentric heat pipe

Major difference of heat pipes is the cross-sectional area of vapor space but there were no difference between each heat pipes. The liquid pressure drop was dominant for capillary limit therefore the cross-sectional area of vapor space had a low effect for heat pipe dry-out phenomenon. Comparison of theoretical capillary limit and experimental results is shown in Figure. 11. Theoretical capillary limit of

annular flow path heat pipe was slightly lower than concentric heat pipe and then both of predictions were underestimated compared to the experimental results.

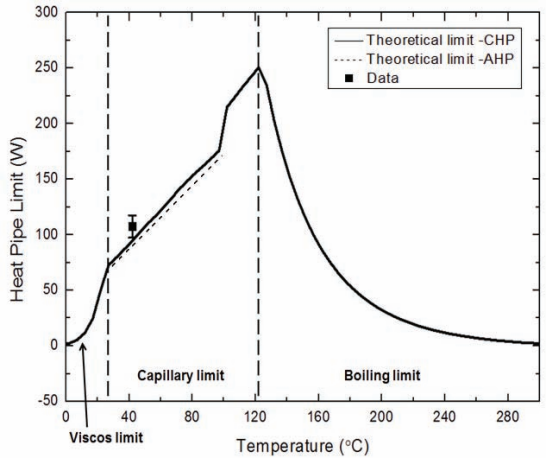


Figure. 11 Comparison of Theoretical capillary limitation and experimental results of concentric heat pipe

## 4. CONCLUSIONS

An experimental study of three 12.7 mm O.D. heat pipes was performed. The working fluid was distilled water, the wick and container material was stainless steel, and the length of heat pipe was 300 mm. The target design was a hybrid heat pipe that serves as a control rod as well. Thermal analyses of annular flow path through the heat pipes were discussed. The objective was to investigate the effects of the inner structure in heat pipe on the heat transfer performance of the hybrid pipe with an annular flow path. An ABS pellet was used instead of a $B_4C$ pellet as the cylindrical structure. The thermal performance of each heat pipe was measured experimentally. Results indicated that the concentric heat pipe design provides the best performance compared to the other designs.

The AEHP design with an annular flow path heat pipe showed heat transfer reduction. The AHP design had increased annular vapor space and cooling surface per unit volume.. The vapor velocity of the AEHP and AHP designs is faster than that of the CHP design. High vapor velocity results in greater friction at the boundary layer interaction between the vapor and liquid flows. The heat transfer coefficient of the AEHP design was relatively small compared to that of the AHP design for equivalent heat flux below the capillary limit. The capillary limit of heat pipe is developed using one dimensional approach. The liquid pressure drop was dominant for capillary limit, thus the cross-sectional area of vapor space had a low effect on heat pipe dry-out phenomenon. Theoretical capillary limit of annular flow path heat pipe was slightly lower than concentric heat pipe and then both of predictions were underestimated compared to the experimental results. It is also confirmed that the annular heat pipe concept of passive decay heat removal works sufficiently.

## NOMENCLATURE

| | | |
|---|---|---|
| $A$ | Area | [$m^2$] |
| $g$ | Acceleration of gravity | [$m/s^2$] |
| $h$ | Heat transfer coefficient | [$W/m^2K$] |
| $l$ | length | [m] |
| $L$ | Latent heat | [J/kg] |
| $\dot{m}$ | Mass flow rate | [kg/s] |
| $\Delta P$ | Pressure difference | [Pa] |
| $Q$ | heat input, power | [W] |
| $\dot{Q}$ | Heat flow rate | [J/s] |
| $q''$ | heat flux | [$kW/m^2$] |
| $r$ | Radius | [m] |
| $R$ | thermal resistance | [°C/W] |
| $T$ | temperature | [°C] |
| $\bar{T}$ | average temperature | [°C] |
| $\rho$ | Density | [$Kg/m^3$] |
| $\varepsilon$ | Fractional void of the wick | [-] |
| $\mu$ | Dynamic viscosity | [Pa·s] |

Subscript

| | |
|---|---|
| a | adiabatic |
| c | condenser |
| c, max | maximum capillary |
| e | evaporator |
| m | maximum |
| eff | effective |
| g | gravity |
| in | input |
| l | liquid |
| o | overall |
| pore | effective pore |
| v | vapor |
| v, e | vapor of evaporator |
| v, a | vapor of adiabatic section |
| v,c | vapor of condenser |
| w | wick |

## ACKNOWLEDGMENTS

This work was supported by the Nuclear Energy Research Program through the National Research Foundation of Korea (NRF) funded by the Ministry of Science, ICT, and Future Planning. (No. 2013M2A8A1041442)

## REFERENCES


1. C. Wang, D. Zhang, S. Qiu, W. Tian, Y. Wu, and G. Su, "Study on the characteristics of the sodium heat pipe in passive residual heat removal system of molten salt reactor", *Nuclear Engineering and Design*, **265**, pp. 691-700 (2013).
2. H. Jouhara, V. Anastasov, and I. Khamis, "Potential of Heat Pipe Technology in Nuclear Seawater Desalination", *Desalination*, **249**, pp. 1055-1061 (2009).
3. M. Mochizuki, T. Nguyen, K. Mashiko, Y. Saito, R. Singh, T. Nguyen, and V. Wuttijumnong, "Prevention Possibility of Nuclear Power Reactor Meltdown by use of Heat Pipes for Passive Cooling of Spent Fuel", *Frontiers in Heat Pipes*, **4** (2013).
4. Singh R, Mochizuki M. "Heat pipe based emergency cooling system for removing decay heat from nuclear reactor and spent fuel pool. In: Japan Association of Heat Pipe Meeting", Waseda, Japan, 09 July, (2011).
5. M. Kole, T.K. Dey, "Thermal performance of screen mesh wick heat pipes using water-based copper nanofluids," *Applied Thermal Engineering*, **50**, pp. 763-770, (2013).
6. S. Schampheleire, K. Kerpel, T. Deruyter, P. Jaeger, M. Paepe, "Experimental study of small diameter fibres as wick material for capillary-driven heat pipes", *Applied Thermal Engineering*, **78**, pp. 258–267, (2015).
7. V. Maziuk, A. Kulakov, M. Rabetsky, L. Vasiliev, M. Vukovic, "Miniature heat-pipe thermal performance prediction tool – software development", *Applied Thermal Engineering*, **21**, pp. 559-571, (2001).
8. A. Faghri, S. Thomas, Performance characteristics of an annular heat pipe, Performance characteristics of a concentric annular heat pipe : Part 1 –Experimental prediction and analysis of the capillary limit, *Transactions of the ASME*, **111**, (1989).
9. A. Faghri, "Heat Pioes : Review, Opportunities and Challenges", *Frontiers in heat pipes*, **5**, (2014).
10. D. H. Kim, S. Y. Park, J. H.Boo , "A Study on the Thermal Performance of Concentric Annular Heat Pipes", *The Korean Society of Mechanical Engineers autumn conference*, pp.1412-1417, (2004)
11. J.H. Boo, S.Y. Park, "An experimental study on the thermal performance of a concentric annular heat pipe", *Journal of mechanical science and technology*, **19**, pp. 1036-1043, (2005).
12. Y. M. Hung, Q. Seng, "Effects of geometric design on thermal performance of star-groove micro-heat pipes", *International Journal of Heat and Mass Transfer*, **54**, pp. 1198-1209, (2011).
13. L. G. Asirvatham, R. Nimmagadda, S. Wongwises, "Heat transfer performance of screen mesh wick heat pipes using silver–water nanofluid", *International Journal of heat and mass transfer*, **60**, pp. 201-209, (2013).
14. X. Yang, Y.Y. Yan, D. Mullen, "Recent developments of lightweight, high performance heat pipes", *Applied Thermal Engineering*, **33**, pp.1-14, (2012).
15. J. Zhang, Y.H. Diao, Y.H. Zhao, X. Tang, W.J. Yu, S. Wang, "Experimental study on the heat recovery characteristics of a new-type flat micro-heat pipe array heat exchanger using nanofluid", *Energy conversion and management*, **75**, pp. 609-616, (2013).
16. K. Shukla, A. Solomon, B. Pillai, B. Singh, S. Kumar, "Thermal performance of heat pipe with suspended nano-particles", *heat mass transfer*, (2012).
17. C.A. Busse, "Pressure drop in the vapour phase of long heat pipes.", *Thermionic Conversion Specialists Conference*,(1967)
18. D. A. Reay, P. A. Kew, heat pipes, *Elsevier*, New York, (2006)